

Article

Mass–Energy Profiles Obtained by Quantum Chemical Computing Applied in Mass Spectrometry: A Case Study with Identification of a Group of Acetalized Monosaccharide Isomers

Carolina Cojocariu^{1,2}, Nicolae Dinca³, Marius Georgescu⁴ , Eugen Sisu¹, Alina Serb^{1,*} 
and Mihai-Cosmin Pascariu^{5,6}

- ¹ Department of Biochemistry and Pharmacology, “Victor Babes” University of Medicine and Pharmacy, RO-300041 Timisoara, Romania; carolina.cojocariu@umft.ro (C.C.); sisueugen@umft.ro (E.S.)
- ² Department of Dental Medicine, Faculty of Dentistry, “Vasile Goldiș” Western University, RO-310414 Arad, Romania
- ³ Department of Technical and Natural Sciences, Faculty of Food Engineering, Tourism and Environmental Protection, “Aurel Vlaicu” University, RO-310330 Arad, Romania; nicolae.dinca@uav.ro
- ⁴ Department of Functional Sciences, “Victor Babes” University of Medicine and Pharmacy, RO-300041 Timisoara, Romania; georgescu.marius@umft.ro
- ⁵ Department of Pharmaceutical Sciences, Faculty of Pharmacy, “Vasile Goldiș” Western University, RO-310414 Arad, Romania; pascariu.cosmin@uvvg.ro
- ⁶ National Institute of Research & Development for Electrochemistry and Condensed Matter, RO-300569 Timisoara, Romania
- * Correspondence: aserb@umft.ro

Abstract: Accurate modeling of small molecules substantially reduces the logistical effort and time consumption to discover and then obtain chemicals with various applications. Molecular stereochemistry is fundamentally involved in the intermolecular interactions that give rise to biological activity. Establishing the configuration of the asymmetric carbon in diastereomers can be decisive in drug design. In the presented analytical technique, on the basis of quantitative structure–fragmentation relationship (QSFR), mass–energy profiles obtained by electron ionization mass spectrometry (EI-MS) for analytes are used, along with some profiles for candidate structures calculated by quantum chemical (QC) methods. Our paper establishes the analytical conditions that lead to the best matching scores of such profiles corresponding to the actual structures for some isomers of acetalized monosaccharides. The optimization was achieved by group validation of five analytes, using four independent variables: the QC method, the descriptor of calculated energy, the impact energy of electrons, and the descriptor of experimental energy. The true structures were obtained using experimental profiles obtained at low electronic impact energies, and profiles were calculated using the DFT (B3LYP/6-31G) and RM1 QC methods. The double quantification of the ionic mass and the energy that generates it, for only a few primary ions of the mass spectrum, even allows the differentiation of acetalized diastereomers.

Keywords: mass–energy profiles; mass spectrometry (MS); quantitative structure–fragmentation relationship (QSFR); molecule recognition; diastereomers



Citation: Cojocariu, C.; Dinca, N.; Georgescu, M.; Sisu, E.; Serb, A.; Pascariu, M.-C. Mass–Energy Profiles Obtained by Quantum Chemical Computing Applied in Mass Spectrometry: A Case Study with Identification of a Group of Acetalized Monosaccharide Isomers. *Appl. Sci.* **2023**, *13*, 7530. <https://doi.org/10.3390/app13137530>

Academic Editor: Andriana Surleva

Received: 24 May 2023

Revised: 19 June 2023

Accepted: 23 June 2023

Published: 26 June 2023



Copyright: © 2023 by the authors. Licensee MDPI, Basel, Switzerland. This article is an open access article distributed under the terms and conditions of the Creative Commons Attribution (CC BY) license (<https://creativecommons.org/licenses/by/4.0/>).

1. Introduction

Accurate modeling of small molecules is a useful starting point in stereochemical structure identification. This approach substantially reduces the logistical and time-consuming effort to discover and then obtain chemicals with various applications. For example, molecular symmetry/asymmetry is essentially involved in the intermolecular interactions that give rise to biological activity. In turn, identifying the configuration of asymmetric carbon atoms in diastereomers may be decisive in structure-based drug design. Recent studies show such investigations, especially those related to the biological interactions of chiral

phytochemicals for the rapid discovery of potential drugs in SARS-CoV-2 [1]. The transfer of the biologically active structure from *in silico* to *in vitro* requires precise analytical methods to discriminate it from its isomers. Quantitative structure–fragmentation relationship (QSFR) techniques based on mass spectrometry could be a solution for controlling the bioactive structure along the entire path from synthesis to its use.

The continuous increase in the number of chemical compounds and their isomers in databases makes their recognition and tracing increasingly subtle and difficult to achieve. Chemical analysis methods must cope with the identification of more and more similar structures to eliminate false-positive candidates. In the case of establishing the isomer symmetry, no orthogonal analytical method is superfluous because only the convergence of as many analytical results as possible can provide structural certainty [2–4].

Chromatography and mass spectrometry (MS) are orthogonal methods of analysis because they are based on different physicochemical processes. The coupling of chromatography with mass spectrometry has offered the possibility of analyzing complex mixtures of analytes [5]. In addition to the classical use of standards, they use new variants of data processing and interpretation, which have been effectively translated to computational molecular simulation approaches [6–8].

In some QSFR analytical techniques using mass–energy profiles in mass spectrometry, the experimental profile resulting from the mass spectrum is compared with the calculated profiles for the candidate structures. Maximum fit for the proper structure should be obtained if the calculated energy descriptors correctly describe the fragmentation [7,8]. For these techniques, the use of elements of the “lock and key” concept of enzymology (E. Fischer) [9] can be intuitive and productive. In this approach, the “lock” would describe the fragmentation mass–energy profile associated with the mass spectrum of the analyte, and the “keys” would be the computed mass–energy profiles for the candidate structures. However, breakdown graphs show that the relativity of ionic intensities in the mass spectrum is in a continuous dynamic depending on the impact energies [10]. Many other factors may influence this relativity. Therefore, it is to be expected that, even for the true structure, the maximum matching of the calculated and experimental mass–energy profiles will be achieved only under certain conditions, or maybe not at all. This situation leads to an analytical impossibility because there are many profiles (keys) that can be calculated for a certain structure; on the other hand, the profile of the lock is not stable, whereby, for a structure, many mass spectra can be obtained, containing different ionic relativities. Another concept in enzymology, “induced fit” (D. Koshland), could provide a solution to this situation by using the matching score of the profiles [9]. Such matching scores can be calculated for all possible key–lock pairs generated by the factors that influence the dynamics of the calculated and experimental profiles. The maximum score should correspond to the actual structure.

Since QSFR techniques have been proven capable of identifying isomers with similar structures and mass spectra [7,8], our study aims to determine if this type of analysis will have good results in the case of some acetalized diastereomers of some monosaccharides. The QSFR technique presented here uses the well-known correlation between enthalpies and Gibbs energies, along with ionic currents (IC), as a tool for mining chemical structures from many calculated mass–energy profiles for the possible structures of the analyte. In the analytical context mentioned above, our study has the following main objectives: (i) the extension of the QSFR analytical technique based on mass–energy profiles to structural isomers and acetalized diastereomers of some monosaccharides; (ii) the simulation of structural analysis for five such isomers using the mining of experimental profiles obtained by mass spectrometry, in the set of quantum chemical (QC)-calculated mass–energy profiles for the candidate structures; (iii) the establishment of the analytical conditions that lead to the best matching scores between the experimental and calculated profiles, such that they indicate the true structures; (iv) the detailed presentation of the chemical structure mining algorithm and the relationship for the calculation of the profile matching score, in order to disseminate this QSFR technique; (v) the validation of QC-calculated mass–

energy profiles for such isomers, located in a database obtained in a previous work [11]. The main novelty of the work is that the mining of isomeric structures is conducted in parallel in two databases with mass–energy profiles, by calculating the matching score. One of the databases was quantum chemically calculated in a previous study [11]. The other was obtained in the present paper from the mass spectrometry analysis of the five isomeric chemical standards. Furthermore, the fulfillment of each of these objectives has an original conception and/or route. The optimization of the technique was achieved by group validation of analytes, a variant frequently used in chromatography because it can simultaneously cover a variety of structures [6,8]. The optimization used four independent variables: the quantum chemical (QC) method, the descriptor of calculated energy, the impact energy (IE) of electrons, and the descriptor of experimental energy. If the mass–energy profiles, calculated and experimental, contain real structural information about the analytes, then the best matching score should correspond to its true positive structures.

2. Materials and Methods

For the validation and optimization of this technique based on QSFR, five structures of acetalized monosaccharides were assigned to the five corresponding chemical standards. For a first stage of optimization and validation of this QSFR technique, the mass–energy profiles calculated for the five candidate structures and the mass–energy profiles resulting from the mass spectra of the respective standards were used. In the absence of a QSFR algorithm for mining chemical structures implemented on personal computers, the group distribution of five analytes to five candidate structures seems feasible from a logistical and time/effort-consuming perspective.

2.1. Calculated Mass–Energy Profiles

Each mass–energy profile consists of a series of pairs of m/z values and energies necessary for the formation of the respective ions. Semiempirical methods such as RM1 and PM7, as well as functional B3LYP, are currently used to calculate the activation energy descriptors of molecular fragmentation in EI-MS, since the fragmentation is an intramolecular transformation. Any other QC method can be used to generate these descriptors because the mining algorithm removes any energy profile that does not provide the maximum docking score. The mass–energy profiles calculated in a previous paper with *HyperChem* 8.0.10, *MOPAC2012*, and *Gaussian 09* software were used (Tables A1–A4) [11–14]. They correspond to structures 1–5 from Figure 1. In these profiles, the strings of the calculated and experimental energy descriptors correspond to the ionic masses in ascending order. In this QSFR-based technique, the calculated energy descriptors were enthalpies and Gibbs energies of ion formation ($\Delta_f H_{ion}$ or $\Delta_f G_{ion}$) and enthalpies and Gibbs energies of fragmentation ($\Delta_f H_{frag}$ or $\Delta_f G_{frag}$), respectively. They were calculated with Equations (1) and (2), respectively:

$$\Delta_f H_{frag} = \Delta_f H (I_i^+) + \sum \Delta_f H (F_i) - \Delta_f H (M), \quad (1)$$

$$\Delta_f G_{frag} = \Delta_f G (I_i^+) + \sum \Delta_f G (F_i) - \Delta_f G (M), \quad (2)$$

where $\Delta_f H (I_i^+)$ is the formation enthalpy of the resulted fragmentation ion, $\sum \Delta_f H (F_i)$ is the sum of the formation enthalpies of accompanying fragments, and $\Delta_f H (M)$ is the molecular enthalpy of candidate structure. The meanings are similar for $\Delta_f G$ [11]

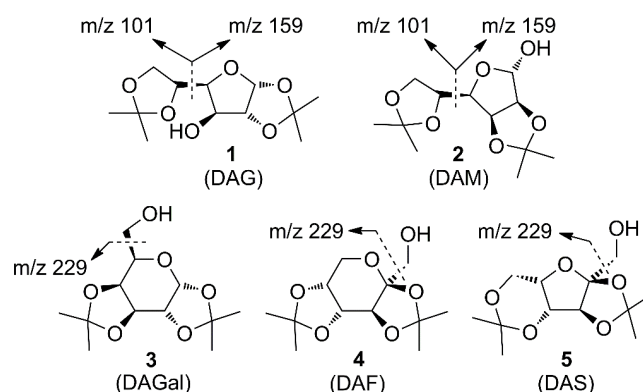


Figure 1. 1,2:5,6-di-*O*-isopropylidene- α -D-glucofuranose (1), 2,3:5,6-di-*O*-isopropylidene- α -D-mannofuranose (2), 1,2:3,4-di-*O*-isopropylidene- α -D-galactopyranose (3), 2,3:4,5-di-*O*-isopropylidene- β -D-fructopyranose (4), and 2,3:4,6-di-*O*-isopropylidene- α -L-sorbofuranose (5).

For ease of reference, they were also assigned the following acronyms: DAG (**d**iacetone-**D**-**g**lucose) (1), DAM (**d**iacetone-**D**-**m**annose) (2), DAGal (**d**iacetone-**D**-**g**alactose) (3), DAF (**d**iacetone-**D**-**f**ructose) (4), and DAS (**d**iacetone-**L**-**s**orbose) (5). Through the perspective of the “Lock and Key” concept, the calculated profiles represent the keys. Each of them contains five of the seven “pins” representing the primary ion energies used in the analysis, possibly obtained from the candidate structures 1–5 in the mass spectrometer (Table 1).

Table 1. The seven predicted primary ions of isomers 1–5.

Primary Ion	Fragmentation
m/z 245	$[M-CH_3\bullet]^+$
m/z 229	See Figure 1
m/z 187	$[M-acetone-CH_3\bullet]^+$
m/z 171	$[M-acetone-HOCH_2\bullet]^+$
m/z 159	See Figure 1
m/z 127	$[M-2\times acetone-HO\bullet]^+$
m/z 101	See Figure 1

The absence of some energy values from the calculated profiles indicates differences in primary fragmentations between the candidate structures. Thus, the ions at m/z 245, m/z 187, and m/z 127 had calculated energies for all structures (1–5). This is because each of them could fragment into those ions by losing methyl, hydroxyl and/or one or two molecules of acetone (Table 1, Figure 1). Instead, several cells in Tables A1–A4 contain the letter “a” for “absent” because the candidate structures could not form the respective primary ions. Thus, the ions at m/z 229 and m/z 171 appeared only for structures 3–5 because they explicitly contain the $-CH_2OH$ group, which the other structures (1 and 2) do not contain (Figure 1, Tables 1 and A1–A4). Similarly, the ions at m/z 159 and m/z 101 appeared only for structures 1 and 2, as they explicitly contain the $-C_5H_9O_2$ group, which the other structures (3–5) do not contain (Figure 1, Tables 1 and A1–A4) [11].

Primary ions result from the cleavage of a single chemical bond from the molecular structure, accompanied or not by the elimination of some small molecules. Their formation requires small fragmentation energies compared to those of ions that are formed after multiple molecular cleavages. If primary ions with the same m/z originate from different molecular structures, they will need different energies for their formation. QC methods were even able to highlight energetic differences, indeed minor, between the mass–energy profiles of some acetalized diastereomers of monosaccharides [11].

2.2. Experimental Mass–Energy Profiles

In the mass spectrometer, each molecule under analysis receives energy that determines the ionization and release of ions, radicals, and smaller molecules (Table 1). The experimental mass–energy profiles are composed of strings of pairs, m/z , and descriptors of the energy consumed in the formation of the respective primary ion.

2.2.1. Reference Standards and Mass Spectrometry

Sugar-based acetals are common substrates in carbohydrate synthesis [15]. De Jongh and Biemann described the relationship between EI mass spectra of *O*-isopropylidene derivatives and their molecular weight, ring size and position, and the stereochemistry of the monosaccharide precursors, thus highlighting the importance of information obtained by such analyses in the structure elucidation and identification of monosaccharides [16]. Working at low energy levels for the molecule ionization offers the advantage of simplifying the mass spectra while providing for a quick examination and interpretation. However, diagnostic ions, which would allow the determination of the structure based on the mass spectrum alone, have not been identified for each of these isomers [17].

Using the commercially (Aldrich and Fluka) available standards 1–5 (Figure 1), 5 mg/mL solutions of these in methylene chloride were prepared. For gas chromatography/mass spectrometry (GC–MS) analysis, a Hewlett Packard HP 6890 Series gas chromatograph, coupled with a Hewlett Packard 5973 mass-selective detector (MSD) system, was used in positive ion mode (calibration factor 1.0). An HP-5 MS capillary column (30 m length, 0.25 mm i.d., 0.25 μ m film thickness) was chosen for the separation step. The temperature program was set up from 100 °C to 250 °C with 15 °C/min; both the injector and the detector temperatures were set at 280 °C, and He was used as the carrier gas. The injection volume was 1 μ L. Ionization energies of 70, 20, 15, 10, and 5 eV were used for the mass spectrometry experiments, with a source temperature of 150 °C. Ionization energy is the most important factor in the optimization of this QSFR technique, because (i) it greatly influences the values of ICs, thus ensuring a large dispersion of the mass–energy profiles, (ii) EI-MS is the biggest consumer of resources and time from the analytic workflow, and must be optimized, and (iii) the 5–70 eV range is accessible to the usual devices with MSD. The MSD was operated in full-scan acquisition mode between m/z 34 and 400 to obtain the total ion chromatogram (TIC). Automatic background subtraction was applied to obtain clean and interference-free mass spectra [17].

2.2.2. Experimental Energy Descriptors

The mass spectrum does not explicitly provide energies. Instead, the energy received by the fragmentable structure, as well as the transformation induced by it, is what establishes the relativity of the IC intensities in the spectrum. High ionic stabilities (describable by enthalpies and Gibbs energies of formation) cause the appearance of large ICs, while high fragmentation activation energies (describable by enthalpies and Gibbs energies of fragmentation) produce small ICs [18]. Although ion intensities are essential in quantitative mass spectrometry, more and more studies use ion intensities to obtain structural information [19,20]. Even in the chemistry of sugars, a recent study used the ratio of ionic intensities for the differentiation of sugar moieties from saponins and to establish their number [21]. The relationship between the energy of the bonds' cleavage during the fragmentation of the analyte and the IC in the spectrum was revealed by numerous equations. They either have a quasi-linear form (Equation (A1)) or a quasi-exponential one (Equation (A2)) [18,22]. Therefore, IC and \ln IC could be useful descriptors of the activation energies for the fragmentations.

2.3. The Matching Score of the Mass–Energy Profiles

The linear correlation function (Pearson) was used to calculate the matching score of the calculated energy descriptors with the experimental ones. This function has already proven its efficiency in the group identification of six positional isomers of tetrachlorinated

biphenyls [8]. Thus, the series of energies calculated for the ions resulting from the primary fragmentation of the candidate structure was compared with the series of energy descriptors (IC or *ln* IC) from the spectrum of the standard. The linear correlation index R_i was, thus, obtained.

The matching of the masses from the calculated and experimental profiles was assessed by the $(n - m_i)/n$ ratio, where n is the number of primary ions used to filter the five candidate structures (seven ions in this case, Table 1), while m_i is the number of mismatches in the sequence of values and, therefore, of empty places in the correlated series of energy descriptors (Tables A1–A5). The difference $(n - m_i)$ represents the number of pairs of energy descriptors that can be formed for the candidate structures and the mass spectra (namely enthalpies and ICs or *ln* ICs pairs) to establish the score. Since $m_i \leq n$, it follows that $(n - m_i)/n$ is a positive subunit number or it has a zero value. In other words, the $(n - m_i)/n$ ratio quantifies the matching of the analyte's primary fragmentation with that of the candidate structure. Thus, the absence of a primary ion from the mass spectrum decreases the matching score. The calculation formula from Equation (1) provides the individual scores in percentages ($P_{i(\%)}$):

$$P_{i(\%)} = 100 \times (1 - R_i \cdot (n - m_i)/n)/2. \quad (3)$$

Since the simulation of the analysis is conducted in a group of five analytes, the score for each variant of structural attribution is the arithmetic mean of five individual scores:

$$P_{(\%)} = (P_1 + \dots + P_5)/5. \quad (4)$$

Equation (3) reduces the matching score if the “key” or “lock” does not contain all the “pins” (energies). Nevertheless, the sequence of candidate structures is not eliminated but only relegated to the list of possible variants. Therefore, Equations (3) and (4) can allow the quantification of calculated and experimental mass–energy profile matching for structural analysis by mass spectrometry. These equations were kept constant throughout the data processing because their optimization was not the subject of this work. Since a commercial application for personal computers that calculates the matching score of the mass–energy profiles has not been developed, we designed accessible worksheets in MS Excel.

2.4. Design of Experiments

The following independent factors were considered for the calculated profiles (Table 2):

- The quantum chemical methods, used in four variants for the calculation of enthalpies ($\Delta_f H$) and Gibbs energies ($\Delta_f G$): RM1, PM7, DFT (B3LYP/6-31G) $\Delta_f H$, and DFT (B3LYP/6-31G) $\Delta_f G$,
- The calculated energy descriptors, in two variants: ($\Delta_f H_{ion}$ or $\Delta_f G_{ion}$) and ($\Delta_f H_{frag}$ or $\Delta_f G_{frag}$), and two independent factors for the experimental profiles (Table 2):
- The descriptors of experimental energy in two variants: IC and *ln* IC,
- The impact energy of electrons on five levels: 5, 10, 15, 20, and 70 eV.

The levels of the independent factors generated $4 \times 2 \times 5 \times 2 = 80$ variants of matching profiles. A list of scores corresponds to each variant. In turn, the score list contains $A_5^5 = 120$ possibilities for distributing the five candidate structures for the five chemical standards. The response factors which followed were the group matching scores ($P_{(\%)}$) and the place (*Rank S*) occupied by the group with the true structures in the descending probability lists. The lists with matching scores allowed the identification of the conditions in which the technique correctly identified the structures.

Matching scores were calculated using Equations (3) and (4). For each standard (as analyte), the column in the matrix with experimental energy descriptor (IC or \ln IC) values is compared with the corresponding column in the matrix with calculated energy descriptor values (Figure 2a,b). In this way, $R_i \times (n - m_i)/n$ and then $P_{(\%)}$ are obtained. This operation is repeated for each of the 120 possible structural assignments. Cells with a green background represent true-positive results, and those with a pink background represent false-positive results. In the optimal analysis conditions, a simple inversion toward the correct structural assignment (e.g., between the DAGal column and the DAM column in the third table in Figure 2a,b, and Supplementary Materials), reduces the matching score of the profiles, and the respective variant is pushed lower in the score list.

3.3. Scores Lists

The score lists bring together all 120 possible distributions of the five candidate structures for the five standards. They are placed in descending order of matching scores, $P_{(\%)}$. One such list was calculated for each of the 80 variants generated by the four variable factors used for optimization. Each list of scores allowed for establishing the maximum probability (P_{max}) and the place (*Rank S*) occupied by the correct distribution of the structures (the cells with green background in Figure 3). The lists (a) and (b) in Figure 3 correspond to the spreadsheets (a) and (b), respectively, from Figure 2 (see also Supplementary Materials).

Standards →	DAF	DAG	DAGal	DAM	DAS	
Rank ↓	Candidate structures ↓					$P_{(\%)}$
1	DAF	DAG	DAGal	DAM	DAS	81.99
2	DAF	DAM	DAGal	DAG	DAS	81.92
3	DAS	DAG	DAF	DAM	DAGal	81.51
4	DAS	DAM	DAF	DAG	DAGal	81.45
5	DAF	DAG	DAS	DAM	DAGal	81.28
6	DAF	DAM	DAS	DAG	DAGal	81.21
7	DAGal	DAG	DAF	DAM	DAS	80.88
8	DAGal	DAM	DAF	DAG	DAS	80.81
9	DAF	DAM	DAG	DAGal	DAS	79.63
10	DAS	DAG	DAGal	DAM	DAF	79.53
11	DAF	DAM	DAG	DAS	DAGal	79.49
12	DAS	DAM	DAGal	DAG	DAF	79.47
13	DAF	DAGal	DAG	DAM	DAS	79.33
14	DAF	DAG	DAGal	DAS	DAM	79.24
15	DAF	DAM	DAGal	DAS	DAG	79.22
16	DAF	DAG	DAM	DAGal	DAS	79.17
17	DAS	DAM	DAG	DAF	DAGal	79.07
18	DAF	DAS	DAG	DAM	DAGal	79.07
19	DAF	DAG	DAM	DAS	DAGal	79.02
20	DAS	DAG	DAF	DAGal	DAM	78.91

(a)

Standards →	DAF	DAG	DAGal	DAM	DAS	
Rank ↓	Candidate structures ↓					$P_{(\%)}$
1	DAF	DAG	DAGal	DAM	DAS	84.52
2	DAGal	DAG	DAF	DAM	DAS	84.43
3	DAF	DAM	DAGal	DAG	DAS	84.32
4	DAGal	DAM	DAF	DAG	DAS	84.24
5	DAS	DAG	DAF	DAM	DAGal	83.59
6	DAS	DAM	DAF	DAG	DAGal	83.39
7	DAS	DAG	DAGal	DAM	DAF	83.28
8	DAF	DAG	DAS	DAM	DAGal	83.09
9	DAS	DAM	DAGal	DAG	DAF	83.08
10	DAF	DAM	DAS	DAG	DAGal	82.89
11	DAGal	DAG	DAS	DAM	DAF	82.69
12	DAGal	DAM	DAS	DAG	DAF	82.49
13	DAGal	DAM	DAG	DAF	DAS	81.10
14	DAF	DAM	DAG	DAGal	DAS	81.09
15	DAGal	DAF	DAG	DAM	DAS	81.03
16	DAF	DAGal	DAG	DAM	DAS	81.04
17	DAF	DAM	DAGal	DAS	DAG	80.66
18	DAGal	DAM	DAF	DAS	DAG	80.58
19	DAS	DAM	DAGal	DAF	DAG	80.59
20	DAS	DAF	DAGal	DAM	DAG	80.52

(b)

Figure 3. Lists with matching scores of mass–energy profiles—the first 20 positions in descending order of $P_{(\%)}$ —in the cases: (a) at 5 eV for \ln IC descriptor and $\Delta_f H_{frag}$ descriptor calculated by RM1 method; (b) at 5 eV for \ln IC descriptor and $\Delta_f G_{frag}$ descriptor calculated by DFT (B3LYP/6-31G) method.

3.4. Validation and Optimization Panel

In Table 3, all 80 pairs of P_{max} and *Rank S* are centralized on the basis of quantum calculation variants. The analysis variant is correct and, therefore, useful only when the maximum matching score is obtained for the true sequence of candidate structures, i.e., P_{max} corresponds to *Rank S* = 1. This situation is fulfilled only in three variants for the independent factors (formatted cells with green background in Table 3):

- The *ln* IC descriptor from the mass spectrum at 5 eV and $\Delta_f G_{frag}$ descriptor calculated using the DFT (B3LYP/6-31G) method (*Rank S* = 1 at P_{max} = 84.52%),
- The *ln* IC descriptor from the mass spectrum at 5 eV and $\Delta_f H_{frag}$ descriptor calculated using the RM1 method (*Rank S* = 1 at P_{max} = 81.99%),
- The *ln* IC descriptor from the mass spectrum at 5 eV and $\Delta_f H_{ion}$ descriptor calculated using the RM1 method (*Rank S* = 1 at P_{max} = 79.20%).

Table 3. The pairs of values for *Rank S* and P_{max} were obtained at validation and optimization of the technique with mass–energy profiles applied in EI-MS for identification of the considered acetalized monosaccharide isomers. Cells with a green background indicate the variants that accurately establish the chemical structures.

Experimental Descriptors →		IC				<i>ln</i> IC			
Calculated Descriptors →		Fragmentation Energy ($\Delta_f H_{frag}$ or $\Delta_f G_{frag}$)		Ionic Energy ($\Delta_f H_{ion}$ or $\Delta_f G_{ion}$)		Fragmentation Energy ($\Delta_f H_{frag}$ or $\Delta_f G_{frag}$)		Ionic Energy ($\Delta_f H_{ion}$ or $\Delta_f G_{ion}$)	
EI	QC	<i>Rank S</i>	P_{max}	<i>Rank S</i>	P_{max}	<i>Rank S</i>	P_{max}	<i>Rank S</i>	P_{max}
5 eV	DFT $\Delta_f G$	9	79.6	6	80.35	1	84.52	4	79.37
10 eV	DFT $\Delta_f G$	5	74.38	102	75.89	19	69.69	113	72.57
15 eV	DFT $\Delta_f G$	14	69.97	114	73.54	62	64.71	114	69.24
20 eV	DFT $\Delta_f G$	17	66.98	114	70.3	15	59.37	78	59.62
70 eV	DFT $\Delta_f G$	13	63.55	115	70.31	15	55.56	90	60.43
5 eV	DFT $\Delta_f H$	7	78.67	6	80.27	2	84.25	4	79.29
10 eV	DFT $\Delta_f H$	8	72.81	102	75.86	15	71.42	113	72.61
15 eV	DFT $\Delta_f H$	30	68.61	113	73.53	45	66.18	114	69.28
20 eV	DFT $\Delta_f H$	46	66.99	113	70.23	20	62.08	78	59.17
70 eV	DFT $\Delta_f H$	33	66.95	113	70.24	26	61.8	86	60.43
5 eV	PM7	22	76.73	5	80.28	3	83.12	3	80.7
10 eV	PM7	3	69.28	86	72.95	5	64.77	106	69.44
15 eV	PM7	2	65.45	110	70.24	35	60.15	110	65.78
20 eV	PM7	4	62.36	110	70.11	1	55.45	92	60.23
70 eV	PM7	4	62.22	110	70.05	1	54.73	93	60.75
5 eV	RM1	3	76.79	2	79.71	1	81.99	1	79.2
10 eV	RM1	6	70.3	101	73.63	27	65.35	114	69.97
15 eV	RM1	17	66.18	115	70.99	94	61.09	115	66.22
20 eV	RM1	13	63.64	115	71.3	12	56.17	116	61.13
70 eV	RM1	13	63.55	115	71.15	15	55.56	116	61.68

The PM7 method can also give *Rank S* = 1 (Table 3, cells with pink background), but the respective variants only happen with a small probability ($\cong 55\%$) when compared with the maximum. Profiles calculated with this method only offer *Rank S* = 3 for P_{max} = 83.12%. Thus, such a quantum method is not useful in a real analysis where the true structure is established only with P_{max} .

The table with the results of the technique's optimization and validation (Table 3) can be considered as a docking panel of the calculated mass–energy profiles with the experimental ones. The maximum docking score (84.52%) correctly indicates the five structures. The optimal conditions of independent factors that can ensure a correct structural analysis show the following:

- There is a tendency to increase the score with decreased electronic impact energy. The best match is performed above the ionization threshold in its vicinity.
- The *ln* IC descriptors offer better results than IC. For this reason, it can be assumed that Equation (A2) is more appropriate to describe the kinetics of dissociation under these optimal conditions.
- The DFT (B3LYP/6-31G) and RM1 quantum calculation methods provide useful values in the description of energy fragmentation profiles of acetalized monosaccharide isomers.
- The $\Delta_f G_{frag}$ and $\Delta_f H_{frag}$ descriptors provide better results than the $\Delta_f H_{ion}$ and $\Delta_f G_{ion}$ descriptors.

This first stage of optimization shows that the precision offered by the new QSFR technique proposed in this work can discriminate between the structural isomers of some acetalized diastereomers of monosaccharides into the group analysis variant. This precision is insufficient for an individual analysis of such a structure. However, the results obtained by the first stage of optimization open perspectives for improving precision through a second stage by shortening the intervals of the analytical factors, increasing the mining resolution in these intervals, improving mass spectrometry, QC methods, descriptors, etc.

4. Discussion

The double quantification of the ionic mass and the energy that generates it for only a few primary ions of the mass spectra allows the differentiation of some structural isomers and acetalized diastereomers of monosaccharides. The increase in the profile matching score at low energy impact agrees with the *quasi-equilibrium theory* (QET) in mass spectrometry. According to QET, the rate constant (k) of a unimolecular reaction is a function of the reactants' excess energy (E) in the transition state. Thus, $k_{(E)}$ strongly depends on the internal energy distribution of any ion. However, there is an upper limit for the rate of dissociation that is defined by the vibrational frequency of the bond to be cleaved [10,23]. Hence, at low impact energy, the excess energy E is small, and the activation energy E_0 of the transition states becomes the main factor that establishes the relativity of the rate constants, $k_{(E)}$, for the primary dissociations (Equations (A1) and (A2)). Under these conditions, an increasing series of E_0 energy descriptors ($\Delta_f H_{frag}$ or $\Delta_f G_{frag}$) corresponds to a decreasing series of $k_{(E)}$ descriptors (IC or \ln IC). As the electronic impact energy increases, the vibrational frequency of the bond to be cleaved becomes an increasingly important factor in determining $k_{(E)}$, thus altering the alignment of the energy profiles. Multiple cleavages and molecule isomerizations before fragmentation in the mass spectrometer can also cover the analytical signal. However, the optimization shows that, at low electronic impact energies, these disturbing factors become insignificant for this variant of this QSFR technique with mass–energy profiles.

After this technique has demonstrated its effectiveness for the group analysis of the considered isomers of acetalized monosaccharides, the next step consists of their identification using the optimal variants established in this paper: $\Delta_f G_{frag}$ and $\Delta_f H_{frag}$ energy descriptors calculated with the quantum DFT (B3LYP/6-31G) and RM1 methods, respectively, and the experimental descriptor \ln IC around the 5 eV impact energy.

5. Conclusions

Both QC computations and EI-MS can generate orthogonal mass–energy profiles, in silico and in vitro, respectively, which can be used to discriminate the chosen isomers of acetalized monosaccharides. The docking with the profile maximum scores in the case of true-positive structures demonstrates the correctness of the data obtained with some QC methods, the EI-MS equipment, and the theories that underpin the ionization–fragmentation process. All the algorithms used in this QSFR technique can be easily implemented on personal computers and constitute important candidates for the development of applications for the automation of chemical analyses. However, a commercial application for personal computers that uses the entire analytical workflow of this QSFR technique has not been developed. Completing the databases of small organic molecules with the computer-generated primary mass–energy profiles, together with the technique of their docking to the experimental profiles presented here, could become a generalized tool for the discrimination of isomeric organic molecules. Furthermore, the QSFR technique presented here, which uses mass–energy profiles generated in silico, along with some generated in vitro by mass spectrometry, can improve the accuracy of the current means of conversion between virtual and real isomeric structures.

Supplementary Materials: The following supporting information can be downloaded at: <https://www.mdpi.com/article/10.3390/app13137530/s1>, File S1: Matching Scores of Mass–Energy Profiles at 5 eV for *ln* IC descriptor and $\Delta_f H_{frag}$ calculated with the RM1 method (a) and the list with matching scores of mass–energy profiles—120 positions in descending order of $P_{(\%)}$ for *ln* IC descriptor and $\Delta_f H_{frag}$ descriptor calculated by RM1 method (b); File S2: Matching Scores of Mass–Energy Profiles at 5 eV for *ln* IC descriptor and $\Delta_f G_{frag}$ descriptor calculated by DFT (B3LYP/6-31G) method (a) and the list with matching scores of mass–energy profiles—120 positions in descending order of $P_{(\%)}$ for *ln* IC descriptor and $\Delta_f G_{frag}$ descriptor calculated by DFT (B3LYP/6-31G) method (b).

Author Contributions: Conceptualization, M.-C.P., N.D., C.C. and A.S.; methodology, M.-C.P., N.D. and E.S.; software, M.-C.P., C.C., N.D. and E.S.; validation, M.-C.P., N.D., E.S., A.S. and M.G.; formal analysis, M.-C.P., N.D., C.C., A.S. and E.S.; investigation, M.-C.P., N.D., C.C., E.S., A.S. and M.G.; resources, C.C. and M.G.; data curation, M.-C.P., N.D., C.C., E.S. and A.S.; writing—original draft preparation, M.-C.P., N.D., C.C., A.S. and M.G.; writing—review and editing, M.-C.P., N.D., C.C., A.S. and M.G.; visualization, N.D., M.-C.P., E.S., A.S. and M.G.; supervision, N.D., M.-C.P., E.S. and M.G.; project administration, M.G., C.C., M.-C.P. and E.S. All authors have read and agreed to the published version of the manuscript.

Funding: Part of this research was conducted at the Center of Genomic Medicine at the “Victor Babes” UMFT (UEFISCDI through POSCCE 185/48749; contract No. 677).

Institutional Review Board Statement: Not applicable.

Informed Consent Statement: Not applicable.

Data Availability Statement: All data are available in this publication (including Appendix A).

Acknowledgments: The authors would like to thank Ramona Curpan and Mircea Mracec from “Coriolan Dragulescu” Institute of Chemistry of the Romanian Academy, and Mihai Medeleanu from Politehnica University Timisoara.

Conflicts of Interest: The authors declare no conflict of interest.

Appendix A

Table A1. $\Delta_f H$ (kcal/mol) database calculated with RM1 [11]. The letter “a” indicates the absence of the respective value.

Structure →	DAF (4)	DAG (1)	DAGal (3)	DAM (2)	DAS (5)
$\Delta_f H(M)$	−283.1	−287.1	−282.6	−288.1	−286.7
$\Delta_f H$ (ion)					
<i>m/z</i> 245	−96.6	−99.6	−97.3	−102.0	−101.8
<i>m/z</i> 229	−46.8	a	−42.4	a	−33.0
<i>m/z</i> 187	−34.2	−39.4	−36.4	−40.2	−4.1
<i>m/z</i> 171	34.5	a	9.6	a	37.0
<i>m/z</i> 159	a	11.7	a	8.8	a
<i>m/z</i> 127	103.7	105.1	87.2	79.4	134.0
<i>m/z</i> 101	a	98.8	a	98.8	a
$\Delta_f H (M \text{ frag}) = \Delta_f H (ion) + \Sigma \Delta_f H (F) - \Delta_f H (M)$					
M → <i>m/z</i> 245	211.4	212.4	210.1	211.0	209.7
M → <i>m/z</i> 229	214.9	a	218.8	a	232.3
M → <i>m/z</i> 187	221.1	219.9	218.3	220.1	254.7
M → <i>m/z</i> 171	243.5	a	218.1	a	249.6
M → <i>m/z</i> 159	a	220.0	a	218.2	a
M → <i>m/z</i> 127	284.1	289.5	267.1	264.9	318.0
M → <i>m/z</i> 101	a	221.1	a	219.8	a

Table A2. $\Delta_f H$ database (kcal/mol) calculated with PM7 [11]. The letter “a” indicates the absence of the respective value.

Structure →	DAF (4)	DAG (1)	DAGal (3)	DAM (2)	DAS (5)
$\Delta_f H(\mathbf{M})$	−277.1	−280.8	−277.7	−281.7	−281.6
$\Delta_f H(\mathbf{ion})$					
<i>m/z</i> 245	−99.4	−102.0	−96.2	−102.1	−100.7
<i>m/z</i> 229	−54.3	a	−41.6	a	−34.0
<i>m/z</i> 187	−37.5	−33.4	−37.7	−38.2	−11.5
<i>m/z</i> 171	13.2	a	40.4	a	36.5
<i>m/z</i> 159	a	14.3	a	14.6	a
<i>m/z</i> 127	109.7	155.7	118.8	87.9	161.6
<i>m/z</i> 101	a	89.9	a	89.9	a
$\Delta_f H(\mathbf{M\ frag}) = \Delta_f H(\mathbf{ion}) + \Sigma \Delta_f H(\mathbf{F}) - \Delta_f H(\mathbf{M})$					
M → <i>m/z</i> 245	205.6	206.7	209.5	207.6	208.8
M → <i>m/z</i> 229	201.5	a	214.8	a	226.2
M → <i>m/z</i> 187	212.1	219.8	212.5	216.0	242.6
M → <i>m/z</i> 171	213.5	a	241.4	a	241.3
M → <i>m/z</i> 159	a	220.5	a	221.6	a
M → <i>m/z</i> 127	283.0	332.8	292.9	265.9	339.5
M → <i>m/z</i> 101	a	215.6	a	213.5	a

Table A3. $\Delta_f H$ database (kcal/mol) calculated with DFT (B3LYP/6-31G) [11]. The letter “a” indicates the absence of the respective value.

Structure →	DAF (4)	DAG (1)	DAGal (3)	DAM (2)	DAS (5)
$\Delta_f H(\mathbf{M})$	−1559.5	−1565.4	−1562.9	−1564.0	−1566.7
$\Delta_f H(\mathbf{ion})$					
<i>m/z</i> 245	−1264.7	−1266.0	−1263.3	−1267.8	−1273.3
<i>m/z</i> 229	−1239.6	a	−1227.6	a	−1237.7
<i>m/z</i> 187	−867.0	−873.4	−870.4	−865.2	−830.3
<i>m/z</i> 171	−827.6	a	−835.4	a	−815.7
<i>m/z</i> 159	a	−728.9	a	−726.2	a
<i>m/z</i> 127	−522.8	−531.4	−534.6	−554.1	−494.5
<i>m/z</i> 101	a	−465.7	a	−465.7	a
$\Delta_f H(\mathbf{M\ frag}) = \Delta_f H(\mathbf{ion}) + \Sigma \Delta_f H(\mathbf{F}) - \Delta_f H(\mathbf{M})$					
M → <i>m/z</i> 245	206.3	211.0	211.0	207.8	204.9
M → <i>m/z</i> 229	213.5	a	228.8	a	222.6
M → <i>m/z</i> 187	210.5	210.0	210.5	216.8	254.4
M → <i>m/z</i> 171	232.0	a	227.5	a	251.1
M → <i>m/z</i> 159	a	229.4	a	230.7	a
M → <i>m/z</i> 127	266.2	263.5	257.8	239.4	301.8
M → <i>m/z</i> 101	a	227.8	a	223.2	a

Table A4. $\Delta_f G$ database (kcal/mol) calculated with DFT (B3LYP/6-31G) [11]. The letter “a” indicates the absence of the respective value.

Structure →	DAF (4)	DAG (1)	DAGal (3)	DAM (2)	DAS (5)
$\Delta_f G(\mathbf{M})$	−1886.7	−1892.7	−1892.1	−1891.0	−1895.0
$\Delta_f G(\mathbf{ion})$					
<i>m/z</i> 245	−1557.9	−1557.4	−1557.3	−1559.4	−1567.4
<i>m/z</i> 229	−1523.3	a	−1510.7	a	−1519.8
<i>m/z</i> 187	−1072.4	−1076.9	−1075.9	−1070.0	−1032.0
<i>m/z</i> 171	−1019.7	a	−1031.1	a	−1005.5

Table A4. Cont.

Structure →	DAF (4)	DAG (1)	DAGal (3)	DAM (2)	DAS (5)
<i>m/z</i> 159	a	−913.0	a	−911.2	a
<i>m/z</i> 127	−654.9	−663.0	−665.1	−686.7	−624.9
<i>m/z</i> 101	a	−591.7	a	−591.7	a
$\Delta_f G (\text{M frag}) = \Delta_f G (\text{ion}) + \Sigma \Delta_f G (\text{F}) - \Delta_f G (\text{M})$					
M → <i>m/z</i> 245	219.4	225.9	225.4	222.2	218.3
M → <i>m/z</i> 229	226.6	A	244.6	a	238.4
M → <i>m/z</i> 187	238.7	240.2	240.7	245.5	287.4
M → <i>m/z</i> 171	264.1	A	258.1	a	286.6
M → <i>m/z</i> 159	a	245.2	a	245.4	a
M → <i>m/z</i> 127	309.1	306.9	304.3	281.6	347.3
M → <i>m/z</i> 101	a	244.7	a	239.6	a

$$k_{(E)} = v \times \left(\frac{E - E_0}{E} \right)^{s-1}, \quad (\text{A1})$$

$$k_{(E)} = v \times e^{-(s-1) \frac{E_0}{E}}, \quad (\text{A2})$$

where k is the rate constant for the dissociation of isolated ions as a function of internal energy, E , and activation energy of the reaction, E_0 , while v is a frequency factor that is determined by the number and density of vibrational states. The exponent is given by the number of degrees of freedom, s , minus 1 for the breaking bond [18].

Table A5. The ICs of primary ions from the mass spectra of the standards (1–5), recorded at 70, 20, 15, 10, and 5 eV. The letter “a” indicates the absence of the respective value.

Ion	DAF 70 eV	DAG 70 eV	DAGal 70 eV	DAM 70 eV	DAS 70 eV
<i>m/z</i> 245	846,208	552,640	813,440	703,872	619,840
<i>m/z</i> 229	211,264	1227	6740	3596	75,632
<i>m/z</i> 187	46,528	246,784	155,456	177,984	125,816
<i>m/z</i> 171	314,560	775	38,872	1329	197,952
<i>m/z</i> 159	815	41,928	1171	11,662	134,144
<i>m/z</i> 127	341,120	231,872	185,664	122,176	96,888
<i>m/z</i> 101	53,168	613,952	54,928	547,136	117,048
Ion	DAF 20 eV	DAG 20 eV	DAGal 20 eV	DAM 20 eV	DAS 20 eV
<i>m/z</i> 245	282,816	403,072	211,520	419,392	638,528
<i>m/z</i> 229	64,576	332	1401	1486	78,920
<i>m/z</i> 187	12,985	179,456	40,480	102,544	106,456
<i>m/z</i> 171	105,728	560	11,025	585	199,744
<i>m/z</i> 159	194	32,104	325	7702	161,472
<i>m/z</i> 127	118,432	158,784	49,808	64,896	79,624
<i>m/z</i> 101	18,488	503,040	16,568	362,240	101,728
Ion	DAF 15 eV	DAG 15 eV	DAGal 15 eV	DAM 15 eV	DAS 15 eV
<i>m/z</i> 245	16,9152	129,848	131,328	186,560	338,880
<i>m/z</i> 229	37,448	a	984	a	39,928
<i>m/z</i> 187	7193	53,656	23,832	42,736	47,264
<i>m/z</i> 171	55,600	a	6233	a	96,712
<i>m/z</i> 159	138	11,515	176	3849	96,440
<i>m/z</i> 127	58,848	51,576	24,688	26,824	37,648
<i>m/z</i> 101	8954	240,512	9001	209,344	55,768

Table A5. Cont.

Ion	DAF 10 eV	DAG 10 eV	DAGal 10 eV	DAM 10 eV	DAS 10 eV
<i>m/z</i> 245	30,072	26,792	41,240	35,904	77,624
<i>m/z</i> 229	6135	a	243	a	8035
<i>m/z</i> 187	894	9062	6175	6425	6633
<i>m/z</i> 171	6110	a	1637	a	13,461
<i>m/z</i> 159	a	1964	50	667	18,224
<i>m/z</i> 127	5320	5395	4504	2574	4274
<i>m/z</i> 101	663	39,784	1730	28,120	6267
Ion	DAF 5 eV	DAG 5 eV	DAGal 5 eV	DAM 5 eV	DAS 5 eV
<i>m/z</i> 245	4520	4604	4083	5921	7360
<i>m/z</i> 229	825	a	a	a	749
<i>m/z</i> 187	a	659	305	523	152
<i>m/z</i> 171	189	a	65	a	319
<i>m/z</i> 159	a	116	a	93	873
<i>m/z</i> 127	96	67	a	71	a
<i>m/z</i> 101	a	1989	56	1616	60

References

- Vicidomini, C.; Roviello, V.; Roviello, G.N. In Silico Investigation on the Interaction of Chiral Phytochemicals from *Opuntia ficus-indica* with SARS-CoV-2 Mpro. *Symmetry* **2021**, *13*, 1041. [CrossRef]
- Vaniya, A.; Fiehn, O. Using fragmentation trees and mass spectral trees for identifying unknown compounds in metabolomics. *Trends Analyt. Chem.* **2015**, *69*, 52–61. [CrossRef]
- Böcker, S.; Dührkop, K. Fragmentation trees reloaded. *J. Cheminform.* **2016**, *8*, 5. [CrossRef] [PubMed]
- Rasche, F.; Scheubert, K.; Hufsky, F.; Zichner, T.; Kai, M.; Svatoš, A.; Böcker, S. Identifying the Unknowns by Aligning Fragmentation Trees. *Anal. Chem.* **2012**, *84*, 3417–3426. [CrossRef] [PubMed]
- Bojin, L.A.; Georgescu, M.; Cojocaru, C.; Pascariu, M.C.; Purcarea, V.L.; Ivan, M.V.; Puiu, M.; Dehelean, C.; Serb, A.F.; Sisu, E.; et al. Structural investigation of raw and modified glycans by MALDI-TOF mass spectrometry. *Farmacia* **2020**, *68*, 891–897. [CrossRef]
- Fedorova, E.; Stavriani, A.; Minenkova, I.; Buryak, A. Calculations of the Thermodynamic Characteristics and Physicochemical Properties of Symmetric and Asymmetric Isomeric Compounds for Identification in Chromatography-Mass Spectrometry. *Symmetry* **2021**, *13*, 1681. [CrossRef]
- Dinca, N.; Covaci, A. Structural identification by differential mass spectrometry as a criterion for selecting the best quantum chemical calculation of formation enthalpy for tetrachlorinated biphenyls. *Rapid Commun. Mass Spectrom.* **2012**, *26*, 2033–2040. [CrossRef] [PubMed]
- Dinca, N.; Dragan, S.; Dinca, M.; Sisu, E.; Covaci, A. New quantitative structure-fragmentation relationship strategy for chemical structure identification using the calculated enthalpy of formation as a descriptor for the fragments produced in electron ionization mass spectrometry: A case study with tetrachlorinated biphenyls. *Anal. Chem.* **2014**, *86*, 4949–4955. [PubMed]
- Tripathi, A.; Bankaitis, V.A. Molecular Docking: From Lock and Key to Combination Lock. *J. Mol. Med. Clin. Appl.* **2017**, *2*, 1–19. [CrossRef]
- Rosenstock, H.M.; Wallenstein, M.B.; Wahrhaftig, A.L.; Eyring, H. Absolute rate theory for isolated systems and the mass spectra of polyatomic molecules. *Proc. Natl. Acad. Sci. USA* **1952**, *38*, 667–678. [CrossRef] [PubMed]
- Pascariu, M.C.; Dinca, N.; Cojocariu, C.; Sisu, E.; Serb, A.; Birza, R.; Georgescu, M. Computed Mass-Fragmentation Energy Profiles of Some Acetalized Monosaccharides for Identification in Mass Spectrometry. *Symmetry* **2022**, *14*, 1074. [CrossRef]
- Hypercube, Inc. HyperChem™ Professional, Version 8.0.10 for Windows; Hypercube, Inc.: Gainesville, FL, USA. Available online: <http://www.hypercubeusa.com/?tabid=360> (accessed on 20 March 2021).
- MOPAC2012; Stewart, J.J.P. Stewart Computational Chemistry, Colorado Springs, CO, USA. Version 15.027W. Available online: <http://OpenMOPAC.net/> (accessed on 20 March 2021).
- Frisch, M.J.; Trucks, G.W.; Schlegel, H.B.; Scuseria, G.E.; Robb, M.A.; Cheeseman, J.R.; Scalmani, G.; Barone, V.; Mennucci, B.; Petersson, G.A.; et al. *Gaussian 09. Revision B.01*; Gaussian, Inc.: Wallingford, CT, USA, 2010.
- Robertson, J.; Stafford, P.M. *Carbohydrates*; Osborn, H.M.I., Ed.; Academic Press: London, UK, 2003; pp. 29–33.
- De Jongh, D.C.; Biemann, K. Mass Spectra of O-Isopropylidene Derivatives of Pentoses and Hexoses. *J. Am. Chem. Soc.* **1964**, *86*, 67. [CrossRef]
- Pascariu, M.C.; Sisu, E.; Ordodi, V.L.; Rusnac, L.M. Spectral Analysis of Diisopropylidenedated Monosaccharides. Low Energy EI-MS Fragmentation Study. *Bul. Stiint. Univ. Politeh. Timis. Ser. Chim. Ing. Mediu.* **2011**, *56*, 6.
- Gross, J. *Mass Spectrometry—A Textbook*, 3rd ed.; Springer: Cham, Switzerland, 2011; pp. 36–40.
- Grimme, S. Towards first principles calculation of electron impact mass spectra of molecules. *Angew. Chem. Int. Ed. Engl.* **2013**, *52*, 6306–6312. [CrossRef] [PubMed]

20. Bauer, C.; Grimme, S. How to Compute Electron Ionization Mass Spectra from First Principles. *J. Phys. Chem. A* **2016**, *120*, 3755–3766. [[CrossRef](#)] [[PubMed](#)]
21. Wang, L.L.; Han, L.F.; Yu, H.S.; Sang, M.M.; Liu, E.W.; Zhang, Y.; Fang, S.M.; Wang, T.; Gao, X.M. Analysis of the Constituents in “Zhu She Yong Xue Shuan Tong” by Ultra High-Performance Liquid Chromatography with Quadrupole Time-of-Flight Mass Spectrometry Combined with Preparative High Performance Liquid Chromatography. *Molecules* **2015**, *20*, 20518–20537. [[CrossRef](#)] [[PubMed](#)]
22. Beynon, J.H.; Gilbert, J.R. Energetics and Mechanisms of Unimolecular Reactions of Positive Ions: Mass Spectrometric Methods. In *Gas Phase Ion Chemistry*; Bowers, M.T., Ed.; Academic Press: New York, NY, USA, 1979; Volume 2, Chapter 13; pp. 153–179.
23. Wahrhaftig, A.L. Ion Dissociations in the Mass Spectrometer. In *Advances in Mass Spectrometry*; Waldron, J.D., Ed.; Pergamon: Oxford, UK, 1959; pp. 274–286.

Disclaimer/Publisher’s Note: The statements, opinions and data contained in all publications are solely those of the individual author(s) and contributor(s) and not of MDPI and/or the editor(s). MDPI and/or the editor(s) disclaim responsibility for any injury to people or property resulting from any ideas, methods, instructions or products referred to in the content.